Proceedings of the 11th Brazilian Congress of Thermal Sciences and Engineering – ENCIT 2006
Braz. Soc. of Mechanical Sciences and Engineering – ABCM, Curitiba, Brazil, Dec. 5-8, 2006

Paper CIT06-0324

THREE DIMENSIONAL SIMULATION OF HEAT TRANSFER WITHIN FURNACES AND REACTOR TUBES FOR THE THERMAL CRACKING OF EDC

Roberto Janny Teixeira Junior
Centro de Tecnologias Ambientais e Energéticas - Instituto de Pesquisas Tecnológicas de São Paulo - IPT. Avenida Prof. Almeida Prado, 532. Cid. Universitária, CEP 05508-901 São Paulo/SP - Brazil.
rjanny@ipt.br

Francisco Domingues Alves de Sousa
Centro de Tecnologias Ambientais e Energéticas - Instituto de Pesquisas Tecnológicas de São Paulo - IPT.
fdasousa@ipt.br

Sandro da Silva Aguiar
Braskem S.A. - Unidade Vinílicos - Pólo Cloroquímico de Alagoas, Marechal Deodoro/AL - Brazil.

Abstract. *This work is an application of the numerical code ERHESICS for thermal behavior simulation of a pyrolysis furnace based on Vinyl Unit of Braskem S/A. This furnace engenders thermal cracking of EDC (ethylene dichloride) into its monomer VCM (vinyl chlorine monomer). ERHESICS aims to predict the effect of operational parameters of wall burners on load's (tubular reactor skin) overall heat flux. To predict thermal performance of a furnace (where thermal radiation's the more significant way of heat transfer), accurate calculus of radiant transfer between combustion products, furnace enclosure and load must be achieved. For Simulation of Brakem's thermal cracking furnace, thermal radiation was approached using Hottel's integral zone method, assuming participant medium as a weighted sum of gray gases. For a known flue gas flow pattern, a coupled simulation of thermal radiation, convection and conduction was carried out. Basic blocks (direct exchange areas) for formulae of zone method were developed specially for rectangular furnaces, using special transformation of variables to reduce computation effort. Exchange areas were computed using a Monte Carlo-like technique. Simulation results were compared to a real case where experimental data's available to verify model predictions. Good accordance was obtained, with maximum relative deviance of 10% from experimental overall heat transfer to tubular reactors skin.*

keywords: *heat transfer, pyrolysis furnace, thermal radiation, zone method, erhesics*

1. Introduction

This work is a result of the development of a computational code (Janny and Sousa, 2005) to predict the effect of operational parameters of natural gas-fired wall burners installed in Braskem's cracking unit F-1401-A. Main parameters changing during furnace's operation would be air excess (i.e. air coefficient) and natural gas flowrate on each burner level – see Fig. (1).

Both effects of total power source provided through all burners and distribution of this source over these burners should be simulated: for a given total power source, which distribution of this source over all burner levels would lead to a increase on load's (tubular reactor skin) overall heat flux, hence greater efficiency. Numerical results would be then used as input to a process modeling software like Aspen Plus®.

The mathematical modeling argued here deals only with furnace region called "radiation chamber" or "radiation section" and, additionally, the following assumptions were made to those of Hottel's work (Hottel and Sarofim, 1967):

i) Steady state condition;
ii) Unidirectional flow with allowance for axial mixing, without secondary flow regions (i.e. recirculation);
iii) Flue gas velocity profile as a sole function of mass flow, temperature and free stream's cross-sectional area;
iv) Flue gas composition along furnace was calculated from imposed air coefficients (air coefficient λ_{air}= [effectively used air]/[stoichiometry air]);
v) Complete fuel conversion (extent of reaction $X = 1$);
vi) Combustion was admitted as punctual phenomena, as if each burner would be replaced by a punctual source of power related to its "injected" fuel flow rate (power $= \dot{m}_{ng} \cdot HHV_{\forall}$, where $\dot{m}_{ng}$ and $HHV_{\forall}$ are flow rate and higher heating value of natural gas, respectively, within control volume $\forall$).

2. Description of the cracking unit

Radiation section has a central plane (symmetry plane) containing 22 reactor tubes, plus 6 reactor tubes on a cross-over plane located on the end of this section. Furnace can be approximated as a prism with rectangular base, whose dimensions (in meters) are: `6.5` height, `1.6` width and `16.7` length.

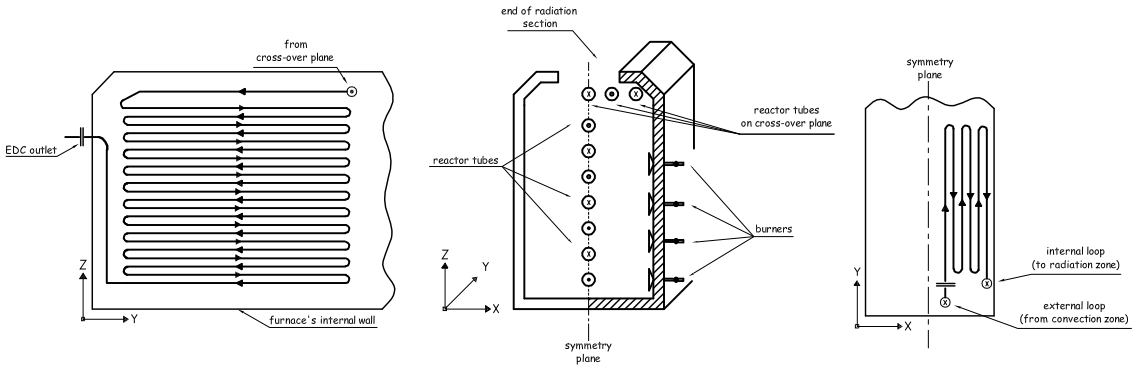

Figure 1: Representation of cracking furnace: load surfaces (reactor tubes) and refractory surfaces (burners)

Heat required for endothermic cracking reaction is provided by means of radiant wall burners located in parallel to the symmetry plane. There're 4 rows (levels) of burners on each side of furnace, each row having 10 burners. These burners provide uniform heat distribution through indirect heating of reactor tubes skin: bulk of radiative heat transfer is due to refractory surfaces (these ones first being heated mainly by burner's flame) emitting and reflecting to reactor tubes. More details about this type of petrochemical furnace may be gathered from John Zink's Handbook (Baukal, 2001).

3. Zoning and discretization

Usually, zone size is dictated by characteristic length scale of conduction and convection (Hottel and Sarofim, 1967). For this problem, convective and conductive heat transfer answer for less than 15% of the overall heat flux to load, therefore a rough furnace zoning, as detailed in Fig. (2), already gives a good description of the problem, and is coherent with experimental data about reactor tube skin temperatures. The present zoning scheme is for one half of furnace, as the problem will be admitted plane-symmetric:

- 5 gas volume zones (V_0,V_1,V_2,V_3,V_4): main gas species are O_2, H_2O, CO_2 and N_2; in the first four volumes (V_0...V_4) there are heat sources (burners); there aren't burners in fifth volume;
- 6 load surface zones (S_2,S_6,S_{10},S_{14},S_{18},S_{20}): discontinued load surfaces composed by spaced tubes and voids; there're strong exchanges by radiation (S_2,S_6,S_{10}, S_{14},S_{18}) and convection (S_{20});
- 16 refractory surface zones (remaining surfaces): made of refractory composites; on some of these surfaces are installed wall burners (S_0,S_4,S_8,S_{12}).

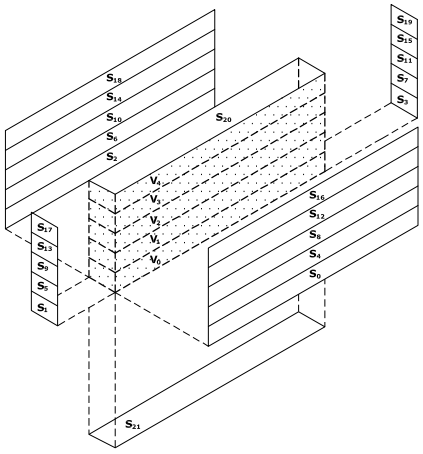

Figure 2: Isometric detail of furnace zoning and identification of all domain zones (surfaces and volumes)

Figure 3 gives a detailed view of unidirectional mass fluxes along volume zones.

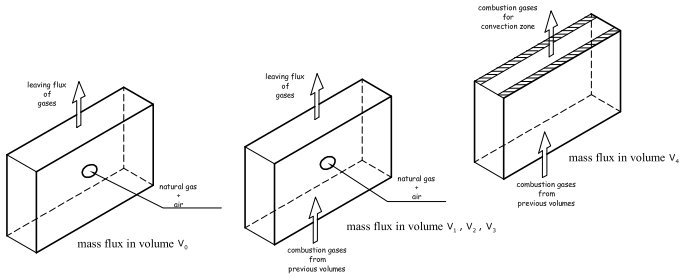

Figure 3: Simplified model for mass flux in each volume zone

4. Zonal analysis

To calculate radiative heat transfer, an integral approach was used employing zonal analysis (Hottel and Sarofim, 1967). Mathematically, the zone method is, perhaps, the simplest numerical quadrature of the differential-integral equation (Radiative Transfer Equation or RTE) governing radiative transfer. Hottel's method make no approximation or assumption to simplify the RTE. By using the concept of radiosity and the principle of energy conservation, this method transforms RTE into a new set of nonlinear algebraic equations.

Together with conventional finite difference techniques to represent convective transports, the zone method provides a way to discretize radiation contribution on a general differential-integral equation.

5. Total balances for zones forming a cavity

Terms related to radiative transport are written as function of exchange factors known as directed flux areas, denoted by $\overrightarrow{GG}$, $\overrightarrow{GS}$, $\overleftarrow{GS}$ and $\overrightarrow{SS}$ for gas-gas, gas-surface, surface-gas and surface-surface exchanges, respectively.

Using the theory developed by Hottel and Sarofim, directed flux areas can be calculated from more fundamental exchange factors, as shown in Tab. (1):

Table 1: Exchange areas used in zone method for radiation analysis (Rhine and Tucker, 1991)

Exchange Factor	**Denomination**	**Function of**
direct exchange area	$\overline{g_i g_j}$, $\overline{g_i s_j}$, $\overline{s_i s_j}$	geometry, gray gas extinction coefficient K.
total exchange area	$\overline{G_i G_j}$, $\overline{G_i S_j}$, $\overline{S_i S_j}$	geometry, K, surface emissivity ϵ_i
directed flux area	$\overrightarrow{G_j G_i}$, $\overleftarrow{G_j G_i}$, $\overrightarrow{G_j S_i}$, $\overleftarrow{G_j S_i}$, $\overrightarrow{S_j S_i}$, $\overleftarrow{S_j S_i}$	geometry, K, ϵ_i, $T_{s,i}$ and $T_{g,i}$ temperatures.

Directed flux areas are computed from total exchange areas, which in turn are computed from direct exchange areas. Using these exchange factors, the transfer of thermal radiation for a particular zone may be incorporated in a total energy balance. In this balance all others heat transfer modes are accounted.

Equations are written for all gas and surface zones, giving rise to a simultaneous system of nonlinear equations. This system can be solved to find temperature and overall heat transferred to each zone.

5.1. Total energy balance for a surface S_i with area A_i

$$\underbrace{\sum_j \overrightarrow{S_j S_i}\ E_{s_j}}_{\text{Incident power over } A_i \text{ resulting of the presence of all emitting surfaces.}} + \underbrace{\sum_k \overrightarrow{G_k S_i}\ E_{g_k}}_{\text{Incident power over } A_i \text{ resulting of the presence of all emitting volumes.}} - \underbrace{A_i\,\epsilon_i\,E_{s_i}}_{\text{Emitted power by } A_i.} + \underbrace{\sum_l h_l A_i\,(T_{g_l} - T_{s_i})}_{\text{Incoming power to } A_i \text{ due to convection.}} = \underbrace{\dot{Q}_{all_{(i)}}}_{\text{Overall power transferred to } A_i.} \qquad (1)$$

Where h_l is a bulk convective heat transfer coefficient and E_{z_j} is the blackbody emissive power at zone's (z_j) temperature, and it's given by Stefan-Boltzmann law ($E_{z_j} = \sigma T_{z_j}^4$).

For surfaces S_2, S_6, S_{10}, S_{14} and S_{20}, $\dot{Q}_{all_{(i)}}$ stands for the overall heat transferred to each $i = 2, 6, 10, 12, 14, 20$ load surface (tubular reactor skin). This is the meaningful quantity to evaluate furnace's efficiency. For refractory surfaces, $\dot{Q}_{all_{(i)}}$ stands for losses by conduction through wall.

5.2. Total energy balance for a gas G_i with volume V_i

$$\underbrace{\sum_k \overrightarrow{G_k G_i}\ E_{g_k}}_{\text{Incident power over } V_i \text{ resulting of the presence of all emitting volumes.}} + \underbrace{\sum_j \overleftarrow{G_i S_j}\ E_{s_j}}_{\text{Incident power over } V_i \text{ resulting of the presence of all emitting surfaces.}} - \underbrace{4\sum_\eta a_{g,\eta} K_\eta\, V_i\, E_{g_i}}_{\text{Emitted power by } V_i.} - \underbrace{\sum_l h_l A_l\,(T_{g_i} - T_{s_l})}_{\text{Leaving power from } V_i \text{ due to convection.}} - \underbrace{\dot{Q}_{e,\,i}}_{\text{Enthalpy variation associated with gases flux within } V_i.} + \underbrace{\mathring{q}_{\forall,\,i}}_{\text{Power source released from combustion reaction in volume } V_i.} = 0 \quad (2)$$

Where

$$\dot{Q}_{\mathbf{e},\,i} = \overrightarrow{\overrightarrow{\Delta}}\,\mathbf{e} \;=\; \sum_{outlet} \left(\dot{m}_{outlet}\ \ \mathbf{e}_{outlet}\right)_i \;-\; \sum_{inlet} \left(\dot{m}_{inlet}\ \ \mathbf{e}_{inlet}\right)_i \quad (3)$$

$$\mathring{q}_{\forall,\,i} = \left(\dot{m}_{gn}\right)_i HHV_\forall \quad (4)$$

In volume V_i, outlet and inlet flowrates (kg/s) for O_2, N_2, CO_2, H_2O are expressed by $\dot{m}_{outlet}$ and $\dot{m}_{inlet}$, respectively. The terms $\mathbf{e}_{outlet}$ and $\mathbf{e}_{inlet}$ – specific enthalpies (kJ/kg) – are calculated at temperatures of volumes V_i and V_{i-1}, respectively. Combustion air is referenced at temperature $T_{ref} = 298K$. Terms $a_{g,\eta}$ and K_η are weight and absorption coefficients, respectively, of the $1, 2, ...\eta$ gray gas.

5.3. Equations system and convergence loop

Generic form of nonlinear equations, to be solved for unknown temperature and heat flux, may be written as bellow.

For total energy balance of m surfaces:

$$\begin{pmatrix} \alpha_{s_{11}} & \alpha_{s_{12}} & \cdots & \alpha_{s_{1m}} \\ \alpha_{s_{21}} & \alpha_{s_{22}} & \cdots & \alpha_{s_{2m}} \\ \vdots & \vdots & \ddots & \\ \alpha_{s_{m1}} & \alpha_{s_{m2}} & \cdots & \alpha_{s_{mm}} \end{pmatrix} \begin{pmatrix} T_{S_1}^4 \\ T_{S_2}^4 \\ \vdots \\ T_{S_m}^4 \end{pmatrix} + \begin{pmatrix} \beta_{s_{11}} & \beta_{s_{12}} & \cdots & \beta_{s_{1m}} \\ \beta_{s_{21}} & \beta_{s_{22}} & \cdots & \beta_{s_{2m}} \\ \vdots & \vdots & \ddots & \\ \beta_{s_{m1}} & \beta_{s_{m2}} & \cdots & \beta_{s_{mm}} \end{pmatrix} \begin{pmatrix} T_{S_1} \\ T_{S_2} \\ \vdots \\ T_{S_m} \end{pmatrix} - \begin{pmatrix} \dot{Q}_{all_{(1)}} \\ \dot{Q}_{all_{(2)}} \\ \vdots \\ \dot{Q}_{all_{(m)}} \end{pmatrix} + \begin{pmatrix} \gamma_{s_1} \\ \gamma_{s_2} \\ \vdots \\ \gamma_{s_m} \end{pmatrix} = \begin{pmatrix} 0 \\ 0 \\ \vdots \\ 0 \end{pmatrix} \quad (5)$$

$$\alpha_{s_{ij}} = \begin{cases} \sigma\left(\overleftarrow{S_i S_i} - A_i \epsilon_i\right), & \text{if } i = j \\ \sigma\ \overleftarrow{S_i S_j}, & \text{if } i \neq j \end{cases} \qquad \beta_{s_{ij}} = \begin{cases} -\sum_k h_k A_i, & \text{if } i = j \\ 0, & \text{if } i \neq j \end{cases}$$

$$\gamma_{s_i} = \sum_l \overrightarrow{G_l S_i}\ T_{g,l}^4 + \sum_k A_i T_{g,k} h_k$$

For total energy balance of n volumes

$$\begin{pmatrix} \alpha_{g_{11}} & \alpha_{g_{12}} & \cdots & \alpha_{g_{1n}} \\ \alpha_{g_{21}} & \alpha_{g_{22}} & \cdots & \alpha_{g_{2n}} \\ \vdots & \vdots & \ddots & \\ \alpha_{g_{n1}} & \alpha_{g_{n2}} & \cdots & \alpha_{g_{nn}} \end{pmatrix} \begin{pmatrix} T_{g_1}^4 \\ T_{g_2}^4 \\ \vdots \\ T_{g_n}^4 \end{pmatrix} + \begin{pmatrix} \beta_{g_{11}} & \beta_{g_{12}} & \cdots & \beta_{g_{1n}} \\ \beta_{g_{21}} & \beta_{g_{22}} & \cdots & \beta_{g_{2n}} \\ \vdots & \vdots & \ddots & \\ \beta_{g_{n1}} & \beta_{g_{n2}} & \cdots & \beta_{g_{nn}} \end{pmatrix} \begin{pmatrix} T_{g_1} \\ T_{g_2} \\ \vdots \\ T_{g_n} \end{pmatrix} + \begin{pmatrix} \gamma_{g_1} \\ \gamma_{g_2} \\ \vdots \\ \gamma_{g_n} \end{pmatrix} = \begin{pmatrix} 0 \\ 0 \\ \vdots \\ 0 \end{pmatrix} \tag{6}$$

$$\alpha_{g_{ij}} = \begin{cases} \sigma \left(\overleftarrow{G_i} G_i - 4 \sum\limits_{\eta} a_{g,\eta} K_\eta \, V_i \right), & \text{if } i = j \\ \sigma \, \overleftarrow{G_i} G_j, & \text{if } i \neq j \end{cases} \qquad \beta_{g_{ij}} = \begin{cases} -\sum\limits_{k} h_k A_k, & \text{if } i = j \\ 0, & \text{if } i \neq j \end{cases}$$

$$\gamma_{g_i} = \sum_{l} \overleftarrow{G_i} S_l \, T_{s,l}^4 + \sum_{k} A_k T_{s,k} h_k - \dot{Q}_{e,\,i} + \overset{\circ}{q}_{\forall,\,i}$$

Systems Eq. (5) and Eq. (6), *a priori*, have $2m + n$ unknowns and only $m + n$ equations. Which means one needs to prescribe m boundary conditions to determinate solutions for those systems. About boundary conditions, see **7. Boundary conditions**.

Briefly, Equation (5) and Eq. (6) were solved by means of a modified Newton-Raphson routine with tuned Powell's functions (Powell, 1970), using trust regions and normalized residues within zero curves of possible solutions. This procedure allowed the nonlinear system to be, relatively, "well behaved" for a given arbitrary initial guess for temperature field.

Convergence loop for computing solution of Eq. (5) and Eq. (6) is shown in Fig. (4).

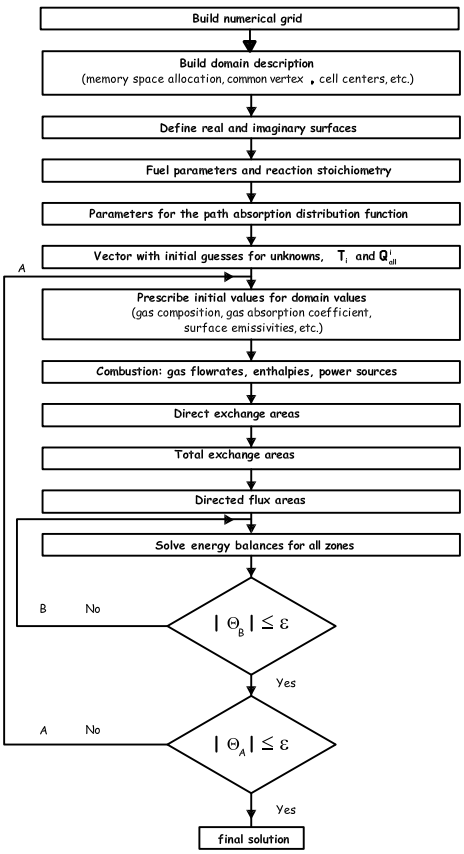

Figure 4: Solution loop of zone method calculus for radiative heat transfer

Inner loop (B) represents the convergence level of an energy balance equation for each zone (for example, equation Eq. (1) for a zone i). Outer loop (A) involves a global convergence, not just including a particular balance, but energy balances for all zones (surfaces and volumes), effects of participant medium absorptivities, direct exchange areas, total exchange areas and directed flux areas.

In Fig. (4), convergence criteria are expressed by Θ_B and Θ_A (here called convergence error) for inner and outer loops, respectively. Some characteristics of convergence stability cannot be inferred only based on the assumption that both source term and radiative intensity are linear with respect to the blackbody intensity of the medium and walls. When the spectral banded nature of absorption and emission phenomena are taken into account (no grey gas assumption), such linearity is not true because of emissivity's dependence of medium and background temperatures.

In this work we propose a expression to monitor convergence based on eigenvalues stability analysis. For example, to measure convergence advance for gas volumes on an outer loop level at $k+1$-th iteration, Equation (7) gives:

$$\Theta_A^{(k+1)} = \chi^{(k+1)} \left(\frac{\chi^{(k+1)}}{\chi^{(k)}} - 1 \right)^{-1} \tag{7}$$

Where $\chi^{(k+1)} = \sqrt{\sum_{i=0}^{n} \left(T_{g,i}^{(k+1)} - T_{g,i}^{(k)} \right)^2}$ is a root mean square (RMS) residual. Figure (5) shows a example for convergence-path measured by Θ_A.

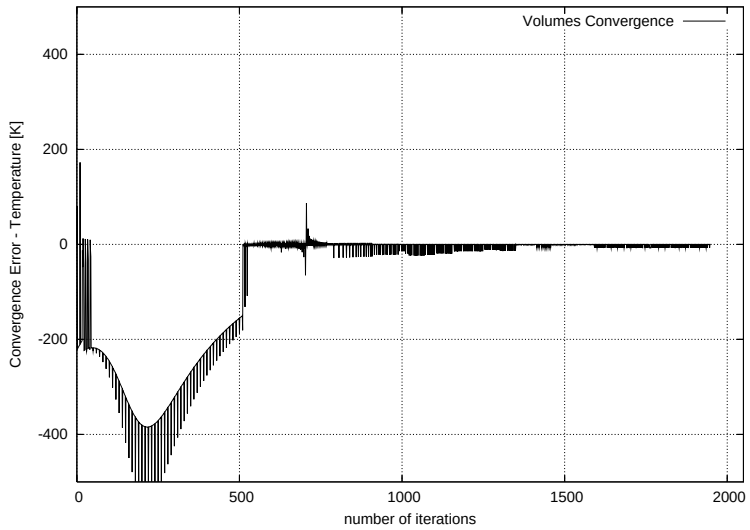

Figure 5: Volume's temperature convergence is mesured by Eq. (7)

A more conventional convergence criteria is applied for Θ_B.

$$\Theta_B^{(k+1)} = \sqrt{\delta T_{g,i}^{(k+1)} \; \delta T_{g,i}^{(k)}} \tag{8}$$

Where $\delta T_{g,i}^{(k+1)} = \left| T_{g,i}^{(k+1)} - T_{g,i}^{(k)} \right|$. Total energy imbalance must be also bellow a target criteria, such as a direct residual $\delta = \sum_{i=0}^{n} \overset{\circ}{q}_{\forall,\, i} - \left(\dot{Q}_{e,\,\mathrm{exit}} + \sum_{j=loads} \dot{Q}_{all_{(j)}} + \text{wall losses} \right)$, where $\dot{Q}_{e,\,\mathrm{exit}}$ is the enthalpy of flue gases at furnace's exit. This way, one could verify if the problem has, in fact, converged.

5.4. Numerical relaxation

Relaxation factors were used in both outer and inner loops, but outer loop was more affected by stability issues. Figure 5 (outer loop's convergence-path measured in terms of Θ_A) shows a progressive damping of Θ_A amplitude, resulting from an adaptive factor relaxation (AFR). Solver allows software's user to change relaxation factor, if needed, after a certain number of iterations or to let itself apply AFR. With the first choice,

user could check, for example, Θ_A and $\delta T_{g,i}$ values and choose suitable relaxation factors to each unknown, dumping iteration instabilities.

One detected source of such instabilities originates from scale differences between terms on Eq. (1) and Eq. (2). In other words, there are terms which are small when compared with some other term with higher magnitude order. For a volume zone total energy balance, specifically, when a great air excess ($\lambda_{ar} > 1.3$) is simulated, the enthalpy term ($\dot{Q}_{e,\,\mathrm{i}}$) becomes, relatively, very big (mainly because of water vapor specific enthalpy). This generates convergence problems in both loops (B and A): for inner loop because of scale differences; and for outer loop because $\dot{Q}_{e,\,\mathrm{i}}$ is an implicit function of temperature.

When AFR is used, different relaxation schemes are applied in loops A and B. For loop B (Newton-Raphson method), solution is iteratively updated accounting to Eq. (9) and Eq. (10). For a zone z_i (either surface or volume)

$$T_{z,i}^{(k+1)} = T_{z,i}^{(k)} + \phi^{(k)}\ \delta T_{z,i}^{(k)} \tag{9}$$

$$\delta T_{z,i}^{(k)} = -\left(J^{(k)}\right)^{-1}\ F\left(T_{z,i}^{(k)}\right) \tag{10}$$

where J is the nonlinear system's Jacobian matrix; ϕ is the relaxation factor; and F is either Eq. (1) or Eq. (2). Factor ϕ is the one (O'Dwyer and O'Donnell, 1995) which minimizes residual L_2 norm in the direction along the solution update, at each iteration (loop B). That is, $\phi^{(k)}$ is chosen as the value which minimizes $\left\|F\left(T_{z,i}^{(k)} + \phi^{(k)}\ \delta T_{z,i}^{(k)}\right)\right\|$ or ensures that $\left\|F\left(T_{z,i}^{(k)} + \phi^{(k)}\ \delta T_{z,i}^{(k)}\right)\right\| < \left\|F\left(T_{z,i}^{(k)}\right)\right\|$. For loop A, Equation (11) was empirically chosen as the relaxation scheme to give best results (great dumping rate and minimum number of iterations needed). Similar method was also proposed by Bastos (Bastos *et al.*, 1995).

$$T_{z,i}^{(k+1)} = (1-\phi_1)\ T_{z,i}^{(k)} + \phi_1\ \left(T_{z,i}^{(k+1)} + \phi_2^{(k)}\ \left(T_{z,i}^{(k+1)} - T_{z,i}^{(k)}\right)\ \sqrt{\frac{T_{z,i}^{(k)}}{T_{z,i}^{(k+1)}}}\ \cdot\right) \tag{11}$$

Equation (11) allows one to choose between two methods: if ϕ_2 (which is an adaptive relaxation factor) is set to 0, this equation simplifies to a traditional under-relaxation method ($0 < \phi_1 \leq 1$); if now $\phi_1 = 1$, only the term under brackets will be evaluated. Of course, if $0 < \phi_1 \leq 1$ and $\phi_2 \neq 0$ a hybrid method will be used (although this case wasn't extensively tested).

The following rules are used to calculate ϕ_2:

i) For each unknown, set a initial $\phi_2^{(0)}$ and define an increment $d\phi$;
ii) For each unknown, calculate $\Delta^{(k-1)} = T_{z,i}^{(k-1)} - T_{z,i}^{(k-2)}$ and $\Delta^{(k)} = T_{z,i}^{(k)} - T_{z,i}^{(k-1)}$;
iii) Calculate the product $\Delta^{(k)} \cdot \Delta^{(k-1)}$;
iv) If the product is negative, oscillation in convergence occurred. In this case set $T_{z,i}^{(k)} = T_{z,i}^{(k-1)}$ and $\phi_2 = \phi_{osc}$;
v) If the product is positive, there wasn't oscillation. In this case set $\phi_2 = \phi_2 + d\phi$.

where ϕ_{osc} is the value affected if the unknown had oscillated, and normally is smaller than $\phi_2^{(0)}$. Unknowns use different relaxation levels determined by their different behavior. Values for $\phi_2^{(0)}$, $d\phi$ and ϕ_{osc} are chosen depending on problem's individuality. Typical values are (Bastos *et al.*, 1995): $\phi_2^{(0)} = -0.6$, $d\phi = 0.05$ and $\phi_{osc} = -0.7$. To solve Eq. (2), an additional under-relaxation scheme (with $\phi_2 = 0$) was utilized to update just the temperature used to calculate $\dot{Q}_{e,\,\mathrm{i}}$, hence minimizing the importance of this term over each iteration.

6. Direct exchange areas for rectangular enclosure

Direct exchange area (DEA) represents the geometric and optic relation between each pair of zones (Hottel and Sarofim, 1967). DEA can also be seen as the energy fraction emitted by an element z_i and absorbed by an element z_j, after a direct transmission – does not include reflection on others surfaces.

Many authors have been applying different methods to calculate DEA for various geometries: Erkku (Erkku, 1959) provided solutions to cylinders and slabs; Vercamen (Vercamen and Froment, 1980) obtained DEAs by calculating photon trajectories using Monte Carlo method.

Works by Erkku (Erkku, 1959), Tucker (Rhine and Tucker, 1991) and Arima (Arima, 1998) related to formulation and calculus of DEA admitted the simplification of an uniform zoning and a fixed range of optical

path lengths (given by $p_g\ L_m$ product, where p_g is the sum of partial pressures of absorbing/emitting gas species and L_m is the mean beam length). In the works by Tucker and Arima, enclosure was approximated by a collection of cubic gas zones bounded by square zone surfaces.

When emissivity and absorptivity of combustion products are represented through use of multiple gray gases, this uniform zoning limits the usage of DEA tables and zone description (size) when high extinction coefficients ($K > 10\ m^{-1}$) are present. In the simulation of cracking furnace F-1401-A, DEAs were formulated for non uniform zones, using special calculus techniques.

Numerical integration of DEA equations were carried out by Monte Carlo statistic method, with an adaptive algorithm (Janny and Sousa, 2005) which evaluates the integrand on a hypercubic region along random directions. The integrand may be seen as radiation beams emitted by a zone which directly arrive on another zone, accounting their interaction with intervenient medium (gases).

6.1. DEA equations

There are three types of DEA: surface-surface ($s_i s_j$), gas-surface ($g_i s_j$) and gas-gas ($g_i g_j$), which can be expressed by the following equations:

$$\overline{s_i s_j} = \int_{A_i} \int_{A_j} \xi\left(A_i, \vec{r}_{ij}\right)\ \tau\left(R\right)\ \frac{cos\left(\theta_i\right)\ cos\left(\theta_j\right)}{\pi\ R^2}\ dA_j\ dA_i \tag{12}$$

$$\overline{g_i s_j} = \int_{V_i} \int_{A_j} \xi\left(V_i, \vec{r}_{ij}\right)\ \tau\left(R\right)\ \frac{K_i\ cos\left(\theta_j\right)}{\pi\ R^2}\ dA_j\ dV_i \tag{13}$$

$$\overline{g_i g_j} = \int_{V_i} \int_{V_j} \xi\left(V_i, \vec{r}_{ij}\right)\ \tau\left(R\right)\ \frac{K_i\ K_j}{\pi\ R^2}\ dV_j\ dV_i \tag{14}$$

where $\tau\left(R\right) = exp\left(-\int_0^R K\left(r\right)\ dr\right)$[1] is the transmittance; $R = \sqrt{\left(x_i - x_j\right)^2 + \left(y_i - y_j\right)^2 + \left(z_i - z_j\right)^2}$ is the absorption path (see Fig. (6)); and $\xi\left(A_i, r_{ij}\right)$ is the characteristic function which accounts for the presence of shadow zones (Janny and Sousa, 2005). Function $\xi\left(A_i, r_{ij}\right) = 1$ when a beam leaving a point $\left(x_i, y_i, z_i\right)$ at surface zone A_i (or volume V_i), locally traveling along a per unit solid angle direction $\vec{r}_{ij}$, is seen when looking from a point $\left(x_j, y_j, z_j\right)$ at the other surface zone A_j (or volume V_j). Otherwise (not seen), $\xi\left(A_i, \vec{r}_{ij}\right) = 0$.

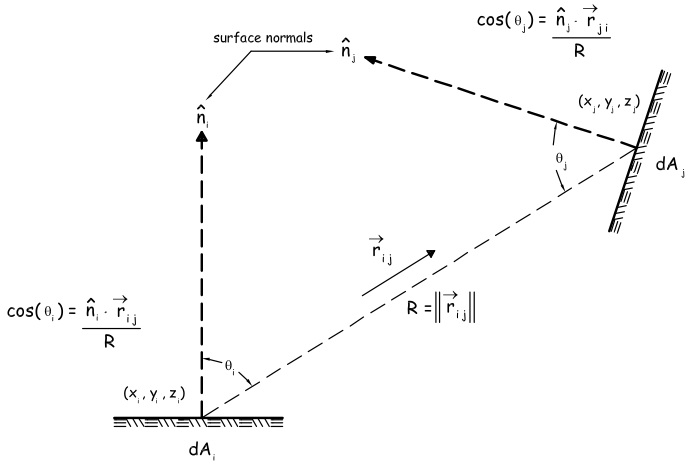

Figure 6: Radiative exchange between two differential surface elements

[1] Instead of fundamental models for transmittance, the exponential law given by Hottel (Hottel and Sarofim, 1967) is used.

Transmittance $\tau\,(R)$ quantifies the energy fraction not transmitted by a radiation beam to the volume zones by which this beam goes through, during a trek from its origin point until its final absorption point. As an approximation, it may be written as

$$\tau(R) \approx \int_{R_{min}}^{R_{max}} exp\left(-\sum_{m} K_{r_m}\ \Delta r_m\right)\ f(R)\,dR \tag{15}$$

where Δr_m is the fraction of total beam length (R) which lies inside a given volume zone with absorption coefficient K_{r_m}. It's calculated based on the intersection of the radiation beam with bounding planes of the volume zone. The factor $f(R)$ is a differential distribution of beam lengths, i.e. the probability that an arbitrarily chosen value of beam length lies between R and $R + dR$ (Vercamen and Froment, 1980). A statistic fit is used because there exist an infinite number of possible absorption paths between a pair of zones.

By example, direct exchange area between a refractory surface and a load surface, without any shadow zones, may be written as (see Fig. (7)):

$$\overline{s_i s_j} = \int_{\overline{x}_i}^{\overline{x}_i+\Delta x_i} \int_{\overline{z}_i}^{\overline{z}_i+\Delta z_i} \int_{\overline{x}_j}^{\overline{x}_j+\Delta x_j} \int_{\overline{z}_j}^{\overline{z}_j+\Delta z_j} \tau\,(R)\ \frac{\overline{y}_j^2}{\pi\ R^4}\ dz_j\ dx_j\ dz_i\ dx_i \tag{16}$$

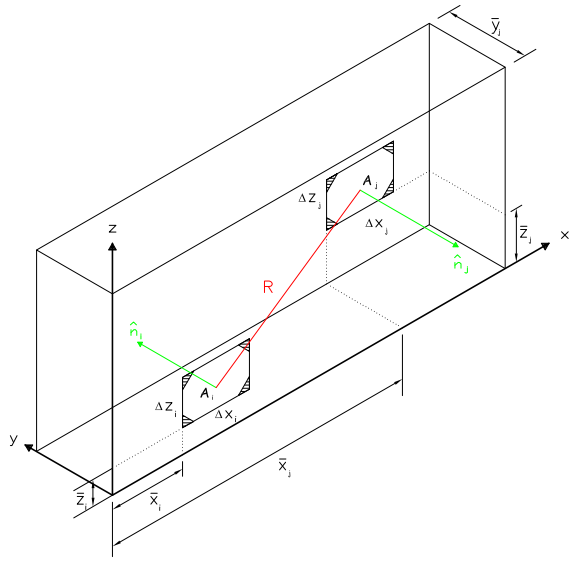

Figure 7: refractory wall zone (A_i) and reactor tube zone (A_j)

6.2. Reduction of the dimension of a multiple integral

A special technique to transform double integral into a sum of simple integrals were developed by Erkku (Erkku, 1959). This technique can be extended to non uniform grids using an additional argument, as proposed by Tian (Tian and Chiu, 2003).

This procedure leads, altogether with the reduction of integral dimension, to a minimization of singularities of function $\overline{s_i s_j}$ within its integration domain. This is a result of great importance, since Eq. (12), Eq. (13) and Eq. (14) have integrands with abrupt variation (singularity) within integration domain for some pair of zones (self radiating or adjacent zones).

7. Boundary conditions

As already mentioned, to solve systems Eq. (1) and Eq. (2) it's necessary to specify m boundary conditions. In the case of the actual zoning of furnace F-1401-A, it'll be prescribed 22 conditions. From these, 6 will be Dirichlet boundary conditions – of first kind, which specifies a value $T = b(x, y, z)$ – prescribed to load surfaces (S_2, S_6, S_{10}, S_{14}, S_{18}, S_{20}). Experimental data from Braskem's DCS (Distributed Control System) provided

information about the temperature of fluid process (inside reactor tube), measured by means of thermocouples allocated immediately upstream (T_{in}) and downstream (T_{out}) from equivalent locations of load surface zones adopted in this work. Starting from arithmetic mean of these values ($(T_{in} + T_{out})/2$), in Tab. (2) tubular reactor skin temperature were calculated accounting for gradients within boundary layer, hence summing a ΔT value to this arithmetic mean.

Table 2: Known (experimental) temperatures of load surfaces

Zone	**Temperature [K]**	**Zone**	**Temperature [K]**
S_2	$T_{S2} = 802$	S_{14}	$T_{S14} = 655$
S_6	$T_{S6} = 767$	S_{18}	$T_{S18} = 579$
S_{10}	$T_{S10} = 732$	S_{20}	$T_{S20} = 542$

The 16 remaining information will be Neumann boundary conditions – of second kind, which specifies a value for $\partial T/\partial \vec{n} = \hat{n} \cdot \nabla T$ – prescribed to refractory surfaces (S_0, S_1, S_3, S_4, S_5, S_7, S_8, S_9, S_{11}, S_{12}, S_{13}, S_{15}, S_{16}, S_{17}, S_{19},S_{21}). In Eq. (2) and Eq. (3), this condition will be associated with term $\dot{Q}_{all}$.

If furnace walls are not admitted adiabatic ($\dot{Q}_{all} = 0$), there will be losses through these walls and $\dot{Q}_{all}$ wont be null. In this case, $\dot{Q}_{all}$ will be iteratively computed in the following way (Janny and Sousa, 2005):

$$\dot{Q}^{(k)}_{\text{all}_{(i)}} = \text{Losses}^{(k)}_{i} = \dot{Q}^{(k)}_{\text{conduction}_{(i)}} = A_i \, \frac{\kappa^{(k)}_i}{\Delta l_i} \left(T^{(k)}_{si} - T^{(k)}_{i,e} \right) \tag{17}$$

$$\left[T^{(k)}_{i,e} \right]^4 + \left(\frac{\Delta l_i \; h^{(k-1)}_{i,e} + \kappa^{(k-1)}_i}{\Delta l_i \; \epsilon^{(k-1)}_{i,e} \; \sigma} \right) T^{(k)}_{i,e} - \frac{\kappa^{(k-1)}_i \; T^{(k-1)}_{si} + \Delta l_i \; h^{(k-1)}_{i,e} \; T_{\infty,e}}{\Delta l_i \; \epsilon^{(k-1)}_{i,e} \; \sigma} = 0 \tag{18}$$

where $T_{i,e}$ is furnace external wall's temperature (adjacent to surface S_i); Δl_i is refractory block thickness (adjacent to surface S_i); κ_i is refractory thermal conductivity (adjacent to surface S_i); $\epsilon_{i,e}$ is furnace external wall's emissivity (adjacent to surface S_i); $h_{i,e}$ is furnace external wall's convection coefficient (adjacent to surface S_i); and $T_{\infty,e}$ is the environment temperature. The quartic Eq. (18) has a known analytic solution.

7.1. Model to represent an array of tubes

A model was developed (Janny and Sousa, 2005) to replace a set of tubes and voids, by a gray plane (in the same averaged temperature of the array of tubes within the discredited zone), whose emissivity is calculated as follows (see Fig. (8)):

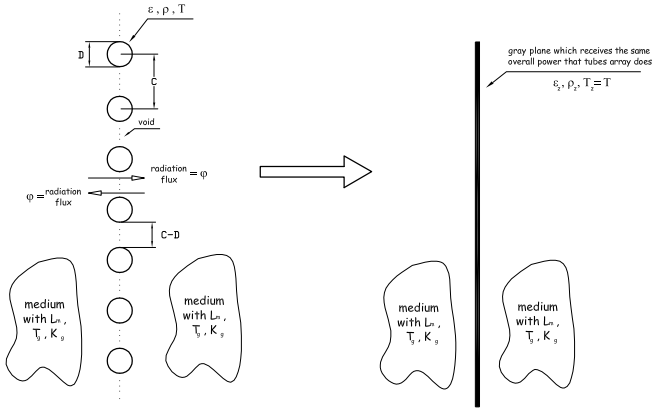

Figure 8: Replacing a set of tubes and voids by a gray plane

$$\epsilon_z = \frac{\epsilon}{\rho} \, \frac{\pi \, D}{2 \, C} \left[\frac{D}{2} \, Y^2 + (C - D)(Y - \pi) \right] \left[\frac{D}{2} \, Y^2 + (C - D) \left(Y - \frac{\pi}{\rho} \right) \right]^{-1} \tag{19}$$

where $Y = arcsin\left(\frac{D}{C}\right) + \left[\left(\frac{C}{D}\right)^2 - 1\right]^{1/2} - \frac{C}{D}$. Assuming symmetric conditions on both sides of furnace, equal amount of radiation which comes from the right side and irradiates over a void with $C - D$ width, also leaves the left side towards right side. Therefore, it's like if the void $C - D$ would reflect all incident radiation. In other words, the void $C - D$ behaves like a reflector ($\epsilon = 0$, $\rho = 1$). Similar procedure is detailed by Hottel (Hottel and Sarofim, 1967).

8. Results

Simulation results are compared with measured experimental data presented in Tab. (3). Operating conditions of furnace are given in Tab. (4).

Table 3: Experimental data from furnace F-1401-A operation

Experimental data	Value
Overall heat transferred to reactor tube skin (both sides of furnace)	9206 [kW]
Overall heat transferred to reactor tube skin (one side)	4603 [kW]
Volume V_0 temperature	1144 [K]
Volume V_2 temperature	1184 [K]
Volume V_3 temperature	1189 [K]
Flue gas temperature at radiation section's exit (V_4)	1062 [K]

Table 4: Furnace F-1401-A operating conditions

Condition	Value (half furnace)	Condition	Value
Fuel flowrate in zone S_0	0.0481 $[kg/s]$	Fuel's carbon content	0.7245
Fuel flowrate in zone S_4	0.0349 $[kg/s]$	Fuel's hydrogen content	0.2323
Fuel flowrate in zone S_8	0.04134 $[kg/s]$	Fuel's sulfur content	0.000
Fuel flowrate in zone S_{12}	0.04134 $[kg/s]$	Fuel's nitrogen content	0.0297
Fuel flowrate in zone S_{16}	0.0 $[kg/s]$	Fuel's oxygen content	0.0135
Air excess	1.05 [air/stoich air]	Fuel's higher heating value	49113 $[kJ/kg]$
Heat input (total)	8137 $[kW]$	Fuel's density	0.7729 $[kg/Nm^3]$

Figure (9) gives the simulation results for predicted temperatures and Fig. (10) gives the predicted overall heat transferred to each load (tubular reactor skin) zone, summing a total of 4375 kW. Hence, a deviation of -4.9% from the value in Tab. (3).

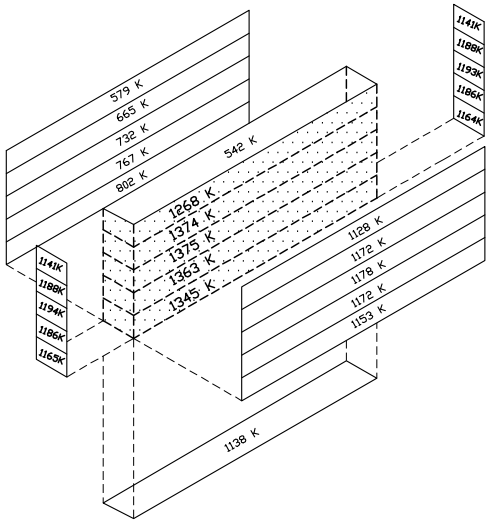

Figure 9: Temperature results from simulation

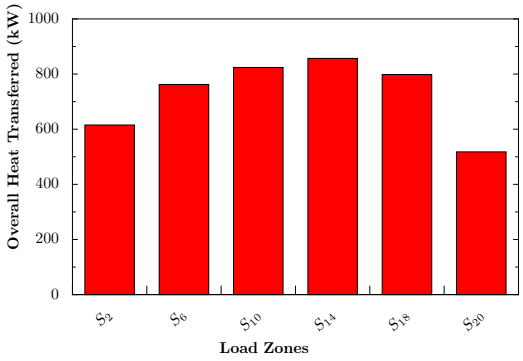

Figure 10: Overall heat transferred to each load surface (simulation result)

The deviation from the experimental overall heat transfer – see Table (5) – is acceptable in terms of mathematical modeling, given the actual simplifications about zoning and flow descriptions.

Table 5: Relative deviations between simulated and experimental temperatures

Volume zone	Experimental value [K]	Simulated value [K]	Deviation [%]
V_0	1144	1345	-17.6
V_2	1184	1375	-16.1
V_3	1189	1374	-15.6
V_4	1062	1268	-19.4

These significant differences between simulated and experimental values are due to many factors related to both mathematical model and furnace operating conditions when measurements were taken:

a) During fieldwork, combustion conditions in all volumes were sub-stoichiometric (CO content in flue gases well over 5000 ppm). In simulated cases, combustion was admitted super-stoichiometric in all volumes ($\lambda_{ar} = 1.05$). This condition results in an overestimation of simulated $T_{g,i}$ $(i = 0, 2, 3, 4)$;

b) Experimental values for volume V_4 temperature were continually measured by a bare thermocouple, inserted into the gas stream immediately before radiation section's exit. Hence allowing thermocouple to "view" much cooler surfaces than gases of the stream where it was inserted. This condition results in a sub-estimation of the experimental value for $T_{g,4}$.

9. References

Arima, M. N., 1998, "Aplicação do Método de Zonas a um Forno de Refino de Cobre", Graduation Project, Escola Politéctica da Universidade de São Paulo, São Paulo.

Bastos, J. A., Ida, N., and Mesquita, R. C., 1995, "A Variable Relaxation Technique in Non-linear Problems", IEEE Transactions of Magnetics, Vol. 31, pp. 1733–1736.

Baukal, C. E., 2001, "The John Zink Combustion Handbook", CRC Press, New York, United States.

Erkku, H., 1959, "Radiant Heat Exchange in Gas-filled Slapbs and Cylinders", PhD thesis, Massachisetts Institute of Technology, Cambridge.

Hottel, H. C. and Sarofim, A. F., 1967, "Radiative Transfer", McGraw-Hill, New York, United States.

Janny, R. and Sousa, F. D. A., 2005, "Simulação Tridimensional do Forno F-1401-A" (Technical Report N°80337-205), Istituto de Pesquisas Tecnologicas de São Paulo - IPT.

O'Dwyer, J. and O'Donnell, T., 1995, "Choosing the Relaxation Parameter for the Solution of Nonlinear Magnetic Field Problems by the Newton-Raphson Method", University of College Dublin.

Powell, M. J. D., 1970, "A Hybrid Method for Nonlinear Equations", Numerical Methods for Nonlinear Algebraic Equations (Gordon and Breach)., pp. 86–114.

Rhine, J. M. and Tucker, R. J., 1991, "Modelling of Gas-Fired Furnaces and Boilers", McGraw-Hill, London, United Kingdom.

Tian, W. and Chiu, W. K. S., 2003, "Calculation of Direct Exchange Areas for Nonuniform Zones Using A Reduced Integration Scheme", ASME Int. J. Heat Transfer, Vol. 125, pp. 839–844.

Vercamen, H. A. J. and Froment, G. F., 1980, "An Improved Zone Method Using Monte-Carlo Techniques for Simulaion of Radiation in Industrial Furnaces", Int. J. Heat Mass Transfer, Vol. 23, pp. 329–337.